Type: Journal Article

Title: Effects of Particle Size and Cushioning Thickness on the Performance of Gabions against Boulder Impact

Su, Y; Cui, Y*; Ng, C. W. W; Choi, C. E.; Kwan, J. S. H.

First-author

Name: Dr. Yuchen Su
Affiliation: JSIT Group
Address: Nanjing 210017, China

Corresponding-author*

Name: Dr. Yifei Cui
Affiliation: Department of Civil and Environmental Engineering, The Hong Kong University of Science and Technology
Address: The Hong Kong University of Science and Technology, Clear Water Bay, Kowloon, Hong Kong
Email: yifeicui@ust.hk

Co-author

Name: Dr. Charles W. W. Ng
Affiliation: Department of Civil and Environmental Engineering, The Hong Kong University of Science and Technology
Address: The Hong Kong University of Science and Technology, Clear Water Bay, Kowloon, Hong Kong

Co-author

Name: Dr. Clarence E. Choi
Affiliation: Department of Civil and Environmental Engineering, The Hong Kong University of Science and Technology
The HKUST Jockey Club Institute for Advanced Study, The Hong Kong University of Science and Technology
HKUST Fok Ying Tung Graduate School, Nansha, China
Address: The Hong Kong University of Science and Technology, Clear Water Bay, Kowloon, Hong Kong

Co-author

Name: Dr. Julian S.H. Kwan

Affiliation: The Geotechnical Engineering Office of the Civil Engineering and Development Department of Hong Kong

Address: Civil Engineering and Development Building, 101 Princess Margaret Road, Kowloon, Hong Kong

Abstract:

Gabion is one of the most commonly used cushioning layer to shield protection structures against boulders entrained in debris flow. Despite the prevalence of gabion, its cushioning performance is highly variable because of the wide range of rock sizes and cushioning thickness that are recommended in the literature. Correspondingly, the dynamic response of gabion cushioning layers varies dramatically. In this study, large-scale pendulum impact tests were used to calibrate a discrete element model. Subsequently, a parametric study was carried out to discern the effects of particle size and cushioning thickness on the impact load and transmitted load exerted by a boulder. Results reveal that as the particle size in the cushioning layer decreases, the force chains collapse more easily, and the expansion angle of strain energy increases. To optimize the performance of a gabion cushioning layer, practitioners should reduce the size of the particles to a normalized particle radius of about 0.1. A normalized particle radius less than 0.2 ensures that the expansion angle of strain energy is large enough, greater than 45^{o} in this study, so as to enable load spreading across the barrier. To eliminate the effects of energy reflecting off the barrier and back to the point of impact, which augments the impact load, the cushioning layer thickness should be greater than three times the radius of the boulder.

Keywords: debris flow boulder impact; gabion; discrete element model; cushioning thickness; particle size;

Introduction

Debris flows pose a serious threat in mountainous regions (Cui et al. 2011). To intercept this hazardous phenomena, structures such as rigid barriers (Lo 2000) are commonly installed in predicted flow paths. In front of these barriers, cushioning materials (ASTRA 2008; GEO 1993) are often installed to attenuate the impact force and to dissipate the impact energy from large boulders in debris flows (Ng et al. 2016). Correspondingly, research is necessary to examine the application of cost-effective and easy-to-construct cushioning materials (GEO 1993) so as to optimize the design of structural countermeasures.

Large-scale pendulum impact tests have been carried out in the literature to investigate the cushioning performance of gabions (Lambert et al. 2009; Lambert et al. 2014; Ng et al. 2016). Findings from these studies demonstrated that the cushioning mechanism responsible for attenuating the impact load is principally governed by the rearrangement and fragmentation of rock particles in the gabion cells (Lambert et al. 2014). Furthermore, the design load on a gabion cushioning layer estimated using the Hertz equation (Kwan 2012) can be reduced by half. More importantly, the transmitted load and load spreading mechanism are highly-variable due to the wide range of rock fragment sizes that are recommended in design guidelines (GEO 1993) and physical model tests (Lambert et al. 2009; 2014; Ng et al. 2016). Moreover, the recommended cushioning thickness is inconsistent in literature (ASTRA 2008; Ng et al. 2016). ASTRA (2008) recommends a minimum cushioning thickness of 0.5 m, while Lambert et al. (2014) and Ng et al. (2016) recommends cushioning thicknesses

of 1m and 2 m, respectively. A summary of the recommended particle sizes and cushioning thickness is given in Table 1.

The finite element method has been used to back-analyze the cushioning performance of cushioning materials (Coelho et al. 2013). These materials included cork and polystyrene, which are easily represented using continuum mechanics. However, the mechanical response of a coarse granular assembly cannot be easily captured using continuum mechanics because of the development and destruction of force chains (Bertrand et al. 2005; Cui et al. 2017a, 2017b). Correspondingly, the discrete element method (DEM) offers a unique approach to model discontinuous materials (Tang et al. 2017; Cui et al. 2018; Kang and Chan 2018), which rely on the development of force chains to control the mechanical response of the material (Peters et al. 2005; Tordesillas et al. 2014).

The formation of force chains during the impact process has been studied using DEM simulations (Bourrier et al. 2008; 2010; Tordesillas et al. 2014; Zhang et al. 2016, 2017). Muthuswamy and Tordesillas (2006) reported that the force chain network is mainly influenced by stresses between particles, packing density of the granular assembly, and degree of polydispersity. Also, shorter force chains form more easily, and have higher strength compared to longer force chains. The differences in the observed behaviour between short and long force chains are mainly because there are fewer potential points of failure in shorter force chains (Anthony and Marone 2005). Generally, the particle size governs the resistance of a granular assembly against impact loads. Furthermore, Zhang et al. (2016) investigated the effects of

particle size on the resulting impact force and the strength of the force chains. Results showed that increasing particle size leads to higher impact force. Furthermore, their results have also demonstrated that the average force chain length increases with particle size.

A cushioning layer that is too thin will enable the boulder to rebound off the structure that is being protected and therefore augment the impact force. This phenomena has been corroborated by Bourrier et al. (2008). More specifically, a compression wave is reflected by the structure under protection back towards the point of impact before the end of the impact process. The reflected energy in turn increases the boulder impact force. The effects of particle shape on boulder rebound have been investigated using the DEM (Nouguier-Lehon et al. 2003; Antony and Kuhn 2004; Bourrier et al. 2008; Bertrand et al. 2005). In particular, Bourrier et al. (2008) simulated the effects of spherical and clumped-shaped particles. Results showed that clumped-shaped particles are less likely to rearrange compared to spherical particles. Correspondingly, force chains do not collapse as easily when the particle shape is irregular.

Although particle shape and particle crushing serve important roles in the cushioning mechanisms of gabions, these effects require introducing additional input parameters, additional calibration, and longer computational times (Bertrand et al. 2005; Breugnot et al. 2016). To acquire a fundamental understanding of the mechanisms of impact for gabions, this paper aims to first discern the effects of particle size and cushioning thickness on the attenuation of the boulder impact force.

Findings from this study serve to optimize the cushioning performance in engineering practice.

Discrete element method

The objective of this numerical study is to understand the mechanisms of interaction between a spherical boulder and a cushioning layer with different thicknesses and particle sizes. The DEM (Cundall and Strack 1979) was adopted to study the dynamic response of a gabion cell subjected to impact. The commercial software Particle Flow Code in three-dimensions PFC^{3D} (Itasca 1999) was used in this study.

The Hertz-Mindlin contact model was adopted in this study. A schematic of this contact law is shown in Fig. 1. This contact model is widely adopted for investigating the interaction between boulders and a granular assembly (Bourrier et al. 2008). The contact model is a nonlinear approximation of Mindlin and Deresiewicz theory (Mindlin and Deresiewicz 1953). The contact law relates both the normal and tangential incremental contact forces dF_{n} *and* dF_{t} to the normal and the tangential incremental displacements du_{n} *and* du_{t}, which are given as follows (Bourrier *et al.* 2008; 2011):

$$dF_{\mathrm{n}} = \frac{3}{2} K_{\mathrm{n}} (u_{\mathrm{n}})^{0.5} du_{\mathrm{n}} \tag{1}$$

$$dF_{\mathrm{t}} = K_{\mathrm{t}} du_{\mathrm{t}} \xi (F_{\mathrm{n}} tan\phi - F_{\mathrm{t}}) \tag{2}$$

where ϕ is the friction angle, which is chosen as 30° and kept constant, $\xi(x)$ is the

Heaviside function where $\xi(x) = 1$ when $x > 0$ and $\xi(x) = 0$ when $x \leq 0$, K_n and K_t are the normal and shear contact stiffness which are calculate as follows:

$$K_n = \frac{2\sqrt{2R_e}G}{3(1-v)} \tag{3}$$

$$K_t = 2\frac{(3G^2(1-v)R_e)^{1/3}}{2-v}F_n^{1/3} \tag{4}$$

where R_e is the effective radius, G is the shear modulus, and v is the Poisson ratio of the granular assembly. The effective radius between two particles is given as follows:

$$R_e = \frac{2R_1R_2}{R_1+R_2} \tag{5}$$

where R_1 and R_2 are the radii of contact for two contacting bodies.

The minimum time step is closely related to the contact model adopted (Cui et al. 2016). During each simulation, the minimum time step Δt is calculated as follows (Itasca, 1999):

$$\Delta t = \sqrt{\frac{m}{K_c}} \tag{6}$$

where m is the mass of a single particle and K_c is the combined stiffness at the contact point. The calculated DEM time step in this analysis was averaged from 1×10^{-7} s to

1×10^{-6} s.

Model calibration

Field test

Results from Ng *et al.* (2016) were used to calibrate the DEM model in this study. In their tests, a boulder with a diameter of 1.16 m and a mass of 2000 kg was constructed using reinforced concrete. This boulder was used to exert an impact load on a 1-m-thick gabion cushioning layer. The diameter of the rock fragments used to fill gabions ranged from 160 mm to 300 mm. An accelerometer was installed at the back of the boulder to measure changes in acceleration of the boulder.

Numerical model setup

The geometries of the gabion cell and he boulder are similar with that from the physical experiments. Figure 2 shows a comparison of the side views of the physical test setup (Ng *et al.* 2016) and the numerical model setup. A concrete boulder with an initial velocity of 8.4 m/s induced an impact force on the gabion cushioning layer, which was modelled using an assembly of particles contained by four walls. Particles were generated under the influence gravity and allowed to stabilize until the average unbalanced forces divided by the average contact forces was smaller than 0.01 or 1%. A new elasto-plastic model with strain hardening behavior was developed by Bertrand et al. (2005) to simulate the mechanical response of gabion baskets. Although previous research suggested coupling between continuous and discrete approaches to simulate the effect of a wire basket (Breugnot et al. 2016). The gabion baskets were

not modelled in this study to enhance computational efficiency. In PFC, a wall has one active side which can interact with the balls. The active side was in contact with the granular assembly forming the gabion, while the inactive side interacted with the boulder. The front wall (Fig. 2b) was generated only to retain the particles and did not interact with the boulder. The particles, with diameters from 160 mm to 300 mm, were evenly distributed within the four walls. A similar simplification by using wall elements to retain the particles was also adopted by Bourrier *et al.* (2011). The friction angle between particles in this study is 30°. For simplicity, no damping was adopted, so energy is dissipated predominantly by grain-to-grain contact stresses. This approach aligns with that reported by Zhang *et al.* (2017) and Bourrier *et al.* (2008). In order to eliminate the effects of the spatial configuration of the particles, simulations were carried out for 100 different boulder impact points and the average of the impact forces and transmitted loads results were taken. Bourrier *et al.* (2008) reports that that minimum impact point number of 100 to ensure reproducibility of results. In this study, 100 impact points were simulated and the minimum distance between two impact points was 0.05 m. A summary of the parameters used in this study is given in Table 2.

Comparisons between measured and computed results

The boulder impact force is calculated using the following equation:

$$F = \sum_{N_c^{(p)}} F_i^{(c,p)} \tag{7}$$

where $N_c^{(p)}$ is the number of contacts between the boulder and the granular assembly,

$F_i^{(c,p)}$ is the contact force which contains normal and tangential components. Index i has a range $i \in \{1,2,3\}$ prescribed for the x, y, and z directions. Figure 3a shows a comparison between the measured and computed boulder impact forces at an impact energy of 70 kJ. The boulder impact force is the product of the acceleration and mass of the boulder. Large fluctuations are observed for both measured and computed curves due to the collapse and formation of force chains (Zhang et al 2016; Zhang et al. 2017). Results also show that the computed maximum boulder impact force is about 10% larger than that of the measured results. This difference may be because particle crushing is not simulated in the numerical model. The plastic deformation induced by particle crushing extends the impact duration and thereby decreases the boulder impact force. More specifically, force chains are more likely to buckle when crushing occurs (Bourrier *et al.* 2008).

The transmitted loads along horizontal direction of the barrier from the field test (Ng *et al.* 2016) were also computed for comparison. The computed loads were measured using square element, which are embedded in the wall (Fig. 4) at the same locations where the load cells are installed in the field tests. The area of each square element is 2250 mm^2. A comparison of the distribution of loads transmitted to the barrier between the field tests and numerical simulations are shown in Fig. 3b. The computed transmitted load at the center of the wall is three times larger compared to the measured transmitted load. This difference may be attributed to the effect of particle crushing, which is not modelled. By neglecting particle crushing, force chains are less likely to collapse, therefore computed transmitted loads are larger.

Numerical simulation plan

A series of numerical simulations, based on the procedures discussed in the full-scale experiments (Ng *et al.* 2016), were carried out to discern the effects of particle size and cushioning thickness. The particle size distribution of the particles comprising the gabion in the DEM model is calibrated against the particle size distribution of the rocks used in the gabions from the physical model tests of Ng *et al.* (2016). The D_{50} of the rock fragments in the gabion in the field is 0.174 m. Therefore, a particle size distribution with particle radii ranging from 0.290 m to 0.058 m was adopted in the DEM model. Furthermore, cushioning thicknesses (T) of 1 m, 2 m and 3 m were investigated (Fig. 5). A summary of the numerical simulations carried out in this study is given in Table 3.

Interpretation of results

Propagation of energy through force chains

The computed test results for particle radii ranging from 0.08 m to 0.15 m at an impact energy level of 70 kJ are used to analyze the propagation of energy in the granular assembly (Fig. 2b). Figure 6 shows a comparison between the boulder impact force and highest compressive stress induced in the force chains. The equations used to calculate the major and minor principle stresses are given in Eqns. 8 and 9 (Peters *et al.* 2005):

$$\sigma_1 = \frac{\sigma_{11} + \sigma_{33}}{2} + \sqrt{(\frac{\sigma_{11} - \sigma_{33}}{2})^2 + (\sigma_{13})^2} \quad (8)$$

$$\sigma_3 = \frac{\sigma_{11} + \sigma_{33}}{2} - \sqrt{(\frac{\sigma_{11} - \sigma_{33}}{2})^2 + (\sigma_{13})^2} \quad (9)$$

where σ_1 is the major principle stress and σ_3 is the minor principle stress, the σ_{ij} are the components of the symmetric part of the particle stress. The convention for tension is positive, meaning that σ_3 is the highest compressive principle stress. The average stress $\bar{\sigma}_{ij}$ in a volume V of material is defined by using that reported by Nicot *et al.* (2013) is shown as follows:

$$\bar{\sigma}_{ij} = \frac{1}{V}\sum_{N_\mathrm{p}} \bar{\sigma}_{ij}{}^{(\mathrm{p})} V^{(\mathrm{p})} = \frac{1}{V}\sum_{N_\mathrm{p}}\sum_{N_\mathrm{c}^{(\mathrm{p})}} \left(x_i^{(\mathrm{c})} - x_i^{(\mathrm{p})}\right) F_j^{(\mathrm{c,p})} \quad (10)$$

where V is the total volume of the material, $\bar{\sigma}_{ij}{}^{(\mathrm{p})}$ is the average stress in a particle (p), $V^{(\mathrm{p})}$ is the volume of the particle (p); N_p is the number of particles in the control volume. $x_i^{(\mathrm{p})}$ and $x_i^{(\mathrm{c})}$ are the coordinates of the centroid and contact points for a particle, respectively; $F_j^{(\mathrm{c,p})}$ is the force acting on a particle (p) at contact (c). $F_j^{(\mathrm{c,p})}$, which includes both the contact normal and shear forces.

The boulder impact force and average particle stress reaches maximum values at the same time (Fig. 6). This indicates that the boulder impact force is entirely borne by the particles in the force chains (Tordesillas *et al.* 2007, 2009, 2014). A force chain is defined as quasi-linear assembly of particles carrying the majority of the load (Campbell 2003; Muthuswamy and Tordesillas 2006). In this study, an algorithm is used to identify force chains based on the approach proposed by Peters *et al.* (2005).

Fluctuations in boulder impact forces and particle stresses are mainly caused by the displacement of particles as new force chains are formed. During the impact process, particle rearrangements cause force chains to collapse and also form new force chains. This stability of the force chains leads to fluctuations in boulder impact force. Details on the relationship between the boulder impact force and the stability of force chains are discussed later.

The kinetic energy of the boulder is transferred to the granular assembly during impact. The propagation of energy occurs as multiple dynamic interactions between individual particles in a granular assembly (Zhang *et al.* 2017). The propagation of energy is examined by analysing the kinetic energy of the boulder (E_b), the kinetic energy of the granular assembly (E_p), the strain energy of the granular assembly (E_s), and energy dissipated via friction in the granular assembly (E_d).

Figure 7 shows changes in energy during the impact process. E_b is 70 kJ and some strain energy of 5 kJ is generated under the influence of gravity. During loading, the boulder impact energy, which transfers to the granular particles, is firstly converted into strain energy. The E_s increases significantly upon impact, reaching peak values of 30 kJ at less than 0.10 s, which occurs only 0.04 s after the maximum boulder impact force is reached at 0.06 s (Fig. 3a). The slight delay is attributed to the propagation of strain energy in the granular assembly. Meanwhile, the increase of strain energy brings about particle rearrangement, which leads to an increase in particle kinetic energy after the computed time of 0.05 s. At the end of the impact process, E_b of the boulder is 3 kJ and the kinetic energy is sustained by the granular

assembly is about 3 kJ. The dissipated energy through frictional contacts is 64 kJ and the stored strain energy is 5 kJ. Changes in energy show that almost all of the kinetic energy of the boulder is transferred to the granular particles, and up to 86 % of the kinetic energy is dissipated through frictional contacts within the granular assembly. These observations on energy transformation are in line with previous numerical studies (Bourrier et al. 2008; Zhang et al. 2016; Zhang et al. 2017).

Figures 8a and 8b show the propagation of strain energy at 0.06 s and 0.10 s, respectively. Green particles represent major principle stresses that are larger than the average principle stress of the entire granular assembly. The direction of the major principle stress from the positive axis is calculated during the impact process as follows (Peters *et al*. 2005):

$$\tan(2\theta) = \frac{2\sigma_{13}}{\sigma_{11} - \sigma_{33}} \tag{11}$$

$R_\mathrm{p}/R_\mathrm{b}$, represents the ratio between average radius of the particles (R_p) forming the cushioning layer and the radius of the boulder (R_b). At 0.06 s, the strain energy initially transfers to the wall and the boulder impact force reaches a maximum (Fig. 8a). This phenomenon is corroborated by the observations reported by Bourrier et al. (2008) where the rebound velocity of the boulder is mainly caused by reflected energy from the rigid barrier when $R_\mathrm{p}/R_\mathrm{b}$ is less than 0.5. Bourrier et al. (2008) reports that a rebounding boulder is attributed to a second supply of energy from the particles after the shockwave is reflected. This indicates that the cushioning thickness

strongly influences the maximum boulder impact force, which depends on the development of force chains between the boulder and the rigid barrier. Zhang et al. (2017) reports that the development and buckling of force chains significantly influences the global shear resistance of the granular assembly. The stronger the force chains, the higher the maximum boulder impact force that is induced, and correspondingly, more lateral spreading of strain energy. Figure 7b shows the propagation of energy at 0.10 s, coinciding with the maximum strain energy. The region of strain energy propagation is characterized using a force chain expansion angle of about 45^0. The volume of particles located near the centre of impact are principally responsible for transferring strain energy compared to the particles around the peripheral of the point of impact (Zhang et al. 2017). The particles in the central part of the cushioning layer are subjected to much higher confinement compared to that of the surrounding particles. Results demonstrate that after the strain energy transfers to the rigid barrier and the boulder impact force reaches its maximum value, the remaining boulder impact energy diffuses laterally as strain energy. This feature leads to higher loads distributed across the rigid barrier. Furthermore, results suggest that the strain energy expansion angle and speed of energy propagation needs to be considered when designing cushioning materials.

Effects of particle size

Bourrier *et al.* (2008) reported that the particle size in a granular assembly plays an important role on the rebound of the boulder. A parametric study was therefore carried

out to investigate the influences of particle size on the propagation of energy and transmission of force to the rigid barrier.

Figure 9a shows the strain energy expansion angle when the boulder impact force reaches its maximum force at about 0.06 s (R_p/R_b equals to 0.1). The approximate fan shape of the strain energy can be characterized using an expansion angle of 60°. This expansion angle is much larger than that for a radius ratio of five (Fig. 8a). This indicates that the expansion angle becomes larger as the particle size decreases with the same cushioning thickness. This observation is because the propagation of force chains not only depends on the thickness of the cushioning layer, but the propagation also depends on the number of contacts. The particle contacts increase as the particle size decrease. A larger amount of particle contacts means that the boulder is resisted by a much wider area of particles. Correspondingly, a reduction in the particle size also leads the more branching points generated from inside the force chain network. Muthuswamy and Tordesillas (2006) reports that more load can be supported by a force chain network with more branching-points. Therefore, the expansion angle of the force chains increases as the particle size decreases. Results also show that the boulder impact force is not only influenced by the stability of force chains, but also the number of force chains that resist the penetration of the boulder. Furthermore, the strain energy does not reach the rigid barrier when the boulder impact force reaches its maximum value (Fig. 9a). Bourrier et al. (2008) also reported similar findings, a compact layer just adjacent to the boulder for radius ratios smaller than 0.17. This observation implies that that the rigid barrier has a less pronounced

effect on the boulder impact force for smaller R_p/R_b where loads spread laterally more easily.

Figures 10a, 10b and 10c show the influences of R_p/R_b on the performance of the cushioning layer and relevant changes in energy. The R_p/R_b is varied from 0.1 to 0.5, which corresponds average particle radii from 0.058 m to 0.290 m. The average particle number per force chain and the force chain length is also shown to highlight the interactions between particles during impact (Figs. 10a and 10b). Results show that the maximum boulder impact force decreases as R_p/R_b increases from 0.10 to 0.20. This is because the expansion angle of the strain energy for R_p/R_b = 0.1 is much larger than R_p/R_b = 0.2 (Figs. 8a and 9a). A larger strain energy expansion angle suggests a larger number of force chains in contact with the boulder. This means that load can more easily be transferred to a other particles without significant particle rearrangement. This in turn results in less plastic deformation and larger boulder impact forces. Similar findings were reported by Muthuswamy and Tordesillas (2006), whereby a force chain network with more branching-points indicates a greater capacity for a material to support more load, since there are more pathways available for the transmission of stress. By contrast, the maximum boulder impact force increases for R_p/R_b from 0.2 to 0.5. This observation is because the maximum boulder impact force is mainly influenced by the force chains between the boulder and rigid barrier (Fig. 8a). The collapse of force chains induces plastic deformation, thereby extending the impact duration and decreasing the maximum boulder impact force. Anthony and Marone (2005) reported that the stability of

individual force chains decreases with the average number of particles which comprise a force chain. This is because force chains with a larger number of particles have a higher likelihood of failure. Furthermore, results show that the average number of particles per force chain decreases from 5.5 to 3.0. More importantly, force chains collapse more easily for a higher radius ratio ($R_\mathrm{p}/R_\mathrm{b} = 0.1$) compared to that of a lower radius ratio ($R_\mathrm{p}/R_\mathrm{b}$= 0.5).

A comparison between Figs. 10a and 10b shows that an increase in the maximum transmitted load on the rigid barrier is larger than the maximum boulder impact force. This phenomenon can be referred as the dynamic amplification effect (Masuya and Kajikawa 1991; Calvetti 1998; Calvetti et al. 2005; Lambert et al. 2009). This effect suggests that the impact force alone is not sufficient to estimate the transmitted force. The average force chain length increases with the radius ratio and the average particle number per force chain decreases with the radius ratio. Both of these features lead to more load transmission to the rigid barrier. In essence, the purpose of a cushioning material is to reduce the transmitted forces on the rigid barrier. Therefore, it is advantageous for practitioners to adopt gabions comprising of smaller particles.

Figure 10c shows the influence of $R_\mathrm{p}/R_\mathrm{b}$ on the maximum strain energy and the frictional energy dissipated. The maximum strain energy is captured at any given time during the impact process, while the dissipated energy is obtained at the end of impact process. Results reveal that the strain energy for $R_\mathrm{p}/R_\mathrm{b}$ = 0.5 is about twice that of $R_\mathrm{p}/R_\mathrm{b}$ = 0.2 because the stability of force chains increases with $R_\mathrm{p}/R_\mathrm{b}$.

Furthermore, the maximum frictional energy for R_p/R_b = 0.2 is 33 % larger compared to that of R_p/R_b = 0.5. Particle rearrangements induced by force chains collapse and the formation of new force chains enhance energy dissipation through shearing. Correspondingly, less energy is dissipated inside a granular assembly with an increasing R_p/R_b and more strain energy is transmitted to the rigid barrier. This coincides with the transmitted load increasing with R_p/R_b.

Effects of cushioning thickness

The maximum boulder impact force occurs at the same time that the strain energy is transferred to the rigid barrier (Fig. 8a). The thickness of the granular assembly therefore plays an important role in reducing the boulder impact force. The thickness of the cushioning layer can be characterized using a thickness ratio T/R_b. This ratio characterises the cushioning thickness of the granular assembly (T) relative to the boulder radius (R_b). Three different T/R_b of 2, 3 and 5 were simulated.

Figure 11a shows the influence of the thickness ratio T/R_b on the maximum boulder impact force for radius ratios varied from 0.1 to 0.5. The differences in the maximum boulder impact forces between thickness ratios of two and three are all larger than 30 %, for radius ratios from 0.2 to 0.5. This trend is because more energy can reflect back to the boulder with a thinner cushioning and therefore a shorter distance to transfer energy. Zhang et al. (2017) also reported that thinner cushioning layers have less capacity for energy dissipation because of lower number of particles and contacts in the granular assembly. Furthermore, in a thicker granular assembly,

the energy reflected from the rigid barrier does not influence the boulder impact force because the impact duration is shorter than the time required for the reflected energy to travel from the barrier and back to the boulder. However, the difference observed in the maximum boulder impact forces between T/R_{b} of two and three increases as $R_{\mathrm{p}}/R_{\mathrm{b}}$increases from 0.1 to 0.2. This is attributed to the different modes of energy propagation as discussed earlier. As the strain energy expansion angle decreases, more load is transmitted to the rigid barrier. Only slight differences are observed between T/R_{b} three and five for $R_{\mathrm{p}}/R_{\mathrm{b}}$ from 0.1 to 0.5. This means if tT/R_{b} exceeds three, the influence of the rigid barrier becomes negligible. Findings suggest that practitioners should adopt a suitable thickness of granular medium such as $T = 3R_{\mathrm{b}}$ so as to improve the overall cushioning performance.

Figure 11b shows the effects of cushioning thickness on the maximum transmitted load. The maximum transmitted load increases with $R_{\mathrm{p}}/R_{\mathrm{b}}$. The increase in load transmission is caused by a decrease in the force chain expansion angle. Furthermore, an increase in cushioning thickness leads to a decrease in the maximum transmitted load. This trend implies that less load is transmitted to the rigid barrier, which is attributed to more energy dissipation over longer travel distances. Compared with the maximum impact load, the maximum transmitted load becomes steady when $T = 5R_{\mathrm{b}}$. This feature is because the maximum transmitted load mainly relies on the number of force chains between the boulder and rigid barrier for $R_{\mathrm{p}}/R_{\mathrm{b}}$ from 0.2 to 0.5. Furthermore, results indicate that the effects of the force chains on the maximum transmitted load decreases with the cushioning thickness. When the

cushioning thickness ratio is larger than five, the maximum transmitted load only increases slightly, implying that the effect of particle size on the maximum transmitted load is negligible when the cushioning thickness is larger than five.

Conclusions

The effects of particle size and cushioning thickness on the performance of gabion cushioning layers were investigated using the discrete element method. Results from this study can be drawn as follows:

a) As the normalized particle radius (R_p/R_b) increase, force chains collapse more easily and the strain energy expansion angle increases. To optimise the performance of a gabion cushioning layer, practitioners should reduce the size of the particles used in gabion cells.

b) Particles with R_p/R_b less than 0.2 ensures that expansion angles of strain energy that are larger than 45^o, which more efficiently spreads load across the entire barrier.

c) A compression wave reflects off the barrier and augments the boulder impact force. To eliminate this effect, the cushioning layer thickness should be larger than three times that of the boulder radius.

Acknowledgements

This paper is published with the permission of the Head of the Geotechnical Engineering Office and the Director of Civil Engineering and Development, the

Government of the Hong Kong Special Administrative Region. The authors would like to acknowledge the financial support from the Theme-based Research Grant T22-603/15N and the General Research Fund 16209717 provided by the Research Grants Council of the Government of Hong Kong SAR, China. The authors are grateful for the financial sponsorship from the National Natural Science Foundation of China (51709052), the Opening Fund of State Key Laboratory of Hydraulics and Mountain River Engineering (SKHL1609), the Hong Kong Jockey Club Charities Trust, and the support of the HKUST Jockey Club Institute for Advanced Study. Finally, the authors are grateful for the financial support by the Hong Kong Jockey Club Disaster Preparedness and Response Institute (HKJCDPRI18EG01).

References

Anthony, J. L., and Marone, C. 2005. Influence of particle characteristics on granular friction. Journal of geophysical research, **110**(B8). doi: 10.1029/2004JB003399.

Antony, S., and Kuhn, M. 2004. Influence of particle shape on granular contact signatures and shear strength: New insights from simulations. International Journal of Solids and Structures, **41**(21): 5863–5870. doi: 10.1016/j.ijsolstr.2004.05.067.

ASTRA. 2008. Effects of rockfall on protection galleries. Federal Roads Office, Swiss.

Bertrand, D., Nicot, F., Gotteland, P., and Lambert, S. 2005. Modelling a geo-composite cell using discrete analysis. Computers and Geotechnics, **32**(8): 564–577. doi: 10.1016/j.compgeo.2005.11.004.

Bourrier, F., Lambert, S., Heymann, A., Gotteland, P., and Nicot, F. 2011. How multi-scale approaches can benefit the design of cellular rockfall protection structures. Canadian Geotechnical Journal, **48**(12): 1803–1816. doi: 10.1139/t11-072.

Bourrier, F., Nicot, F., and Darve, F. 2008. Physical processes within a 2D granular layer during an impact. Granular Matter, **10**(6): 415–437. doi: 10.1007/s10035-008-0108-0.

Bourrier, F., Nicot, F., and Darve, F. 2010. Evolution of the micromechanical properties of imp acted granular materials. Comptes Rendus Mecanique, **338**(10): 639–47. doi: 10.1016/j.crme.2010.09.007.

Breugnot, A., Lambert, S., Villard, P., and Gotteland, P. 2016. A discrete/continuous coupled approach for modelling impacts on cellular geostructures. Rock Mechanics Rock Engineering, **49**(5): 1831–1848. doi: 10.1007/s00603-015-0886-8.

Calvetti, F. 1998. Distinct element evaluation of the rock-fall design load for shelters, Rivista Italiana di Geotecnica, 32: 63–83.

Calvetti, F., Prisco, C., and Vecchiotti, M. 2005. Experimental and numerical study of rock-fall impacts on granular soils. Rivista Italiana di Geotecnica, 4: 95–109.

Campbell, C.S. 2003. A problem related to the stability of force chains. Granular Matter, **5**(3): 129–134. doi: 10.1007/s10035-003-0138-6.

Coelho, R.M., Alves de Sousa, R.J., Fernandes, F.A.O., and Teixeira-Dias, F. 2013. New composite liners for energy absorption purposes. Materials and Design, **43**: 384–392. doi: 10.1016/j.matdes.2012.07.020.

Cui, P., Hu, K., Zhuang, J., Yang, Y., and Zhang, J. 2011. Prediction of debris-flow danger area by combining hydrological and inundation simulation methods. Journal of Mountain Science, **8**(1): 1–9. doi: 10.1007/s11629-011-2040-8.

Cui, Y., Chan, D., and Nouri, A. 2017a. Discontinuum Modeling of Solid Deformation Pore-Water Diffusion Coupling. International Journal of Geomechanics, **17**(8): 04017033. doi: 10.1061/(ASCE)GM.1943-5622.0000903.

Cui, Y., Chan, D., Nouri, A. 2017b. Coupling of Solid Deformation and Pore Pressure for Undrained Deformation – a discrete Element Method Approach. International Journal for Numerical and Analytical Methods in Geomechanics. **41**(18): 1943–1961. doi: 10.1002/nag.2708.

Cui, Y., Choi, C. E., Liu, L. H. D., and Ng, C. W. W. 2018. Effects of particle size of mono-disperse granular flows impacting a rigid barrier. Natural Hazards. **91**(3): 1179–1201. doi: 10.1007/s11069-018-3185-3

Cui, Y., Nouri, A., Chan, D., and Rahmati, E. 2016. A new approach to the DEM simulation of sand production. Journal of Petroleum Science and Engineering, **147**: 56–67. doi: 10.1016/j.petrol.2016.05.007.

Cundall, P.A., and Strack, O.D.L. 1979. The development of constitutive laws for soil using the distinct element method. In: Proceedings of the 3rd Numerical Methods in Geomechanics, Aachen, Germamny.

Effeindzourou, A., Giacomini, A., Thoeni, K., and Sloan, S. W. 2017. Numerical Investigation of Rockfall Impacts on Muckpiles for Underground Portals. Rock Mechanics and Rock Engineering, **50**(6): 1569–1583. doi: 10.1007/s00603-017-1183-5.

Geotechnical Engineering Office. 1993. Guide to Retaining Wall Design (Geoguide 1). Geotechnical Engineering Office, HKSAR.

Heymann, A., Collombet, M., Lambert, S., and Gotteland, P. 2011. Use of external testing methods to assess damage on rockfall protection structures. Applied Mechanics and Materials, **82**: 704–709. doi: 10.4028/www.scientific.net/AMM.82.704.

Itasca. 1999. PFC 3D-user manual. Minneapolis: Itasca Consulting Group.

Kang, C., and Chan, D. 2018. Numerical simulation of 2D granular flow entrainment using DEM. Granular Matter, **20**(13). doi: 10.1007/s10035-017-0782-x

Kwan, J.S.H. 2012. Supplementary Technical Guidance on Design of Rigid Debris-resisting Barriers. GEO Report No. 270, Geotechnical Engineering Office, HKSAR.

Lambert, S., Gotteland, P., and Nicot, F. 2009. Experimental study of the impact

response of geocells as components of rockfall protection embankments. Natural Hazards and Earth System Sciences, **9**(2): 459–467. doi:10.5194/nhess-9-459-2009.

Lambert, S., Heymann, A., Gotteland, P., and Nicot, F. 2014. Real-scale investigation of the kinematic responses of a rockfall protection embankment. Natural Hazards and Earth System Sciences, **14**(5): 1269–1281. doi:10.5194/nhess-14-1269-2014.

Lo, D.O.K. 2000. Review of natural terrain landslide debris-resisting barrier design. GEO Report No. 104, Geotechnical Engineering Office, HKSAR.

Masuya, H., and Kajikawa, Y. 1991. Numerical analysis of the collision between a falling rock and a cushion by distinct element method, Computer Methods and Advances in Geomechanics, Beer, Booker, and Carter, Balkema, Rotterdam, The Netherlands, 493–498.

Ng, C.W.W., Choi, C.E., Su, A.Y., Kwan, J.S.H. and Lam, C. 2016. Large-scale successive impacts on a rigid barrier shielded by gabions. Canadian Geotechnical Journal, **53**(10): 1688-1699. doi: 10.1139/cgj-2016-0073.

Nicot, F., Hadda, N., Guessasma, M., Fortin, J., and Millet, O. 2013. On the definition of the stress tensor in granular media. International Journal of Solids and Structures, **50**(14–15): 2508–2517. doi: 10.1016/j.ijsolstr.2013.04.001.

Nouguier-Lehon, C., Cambou, B., and Vincens, E. 2003. Influence of particle shape and angularity on the behaviour of granular materials: A numerical analysis. International Journal for Numerical and Analytical Methods in Geomechanics,

27(14):1207–1226. doi: 10.1002/nag.314.

Mindlin, R.D., and Deresiewicz, H. 1953. Elastic spheres in contact under varying oblique forces. Journal of Applied Mechanics, **20**: 327–344. doi: 10.1007/978-1-4613-8865-4_35.

Muthuswamy, M., and Tordesillas, A. 2006. How do interparticle contact friction, packing density and degree of polydispersity affect force propagation in particulate assemblies? Journal of Statistical Mechanics: Theory and Experiment, 2006: P09003. doi: 10.1088/1742-5468/2006/09/P09003.

Peters, J. F., Muthuswamy, M., Wibowo, J., and Tordesillas, A. 2005. Characterization of force chains in granular material. Physical review, **72**(4): 041307. doi: 10.1103/PhysRevE.72.041307.

Tang, Y., Chan, D. H., and Zhu, D. Z. 2017. A coupled discrete element model for the simulation of soil and water flow through an orifice. International Journal for Numerical and Analytical Methods in Geomechanics, **41**(14): 1477-1493. Doi: 10.1002/nag.2677.

Tordesillas, A. 2007. Force chain buckling, unjamming transitions and shear banding in dense granular assemblies. Philosophical Magazine, **87**(32): 4987–5016. doi: 10.1080/14786430701594848.

Tordesillas, A., Steer, C.A.H., and Walker, D.M. 2014. Force chain and contact cycle evolution in a dense granular material under shallow penetration. Nonlin. Processes Geophys, **21**(2): 505–519. doi: 10.5194/npg-21-505-2014.

Tordesillas, A., Zhang, J., and Behringer, R. 2009. Buckling force chains in dense granular assemblies: Physical and numerical experiments. Geomechanics and Geoengineering: An International Journal, **4**(1): 3–16. doi: 10.1080/17486020902767347.

Zhang, L., Lambert, S., and Nicot, F. 2017. Discrete dynamic modelling of the mechanical behaviour of a granular soil. International Journal of Impact Engineering, **103**: 76–89. doi: 10.1016/j.ijimpeng.2017.01.009.

Zhang, L., Nguyen, N.G.H., Lambert, S., Nicot, F., Prunier, F., and Djeran-Maigre, I. 2016. The role of force chains in granular materials: from statics to dynamics. European Journal of Environmental and Civil Engineering, **21**(7–8): 847–895. doi: 10.1080/19648189.2016.1194332.

Figure Captions

Fig. 1. Contact law of Hertz-Mindlin model.

Fig. 2. Side view of test setup: (a) Physical test (Ng *et al.* 2016); (b) Numerical simulation

Fig. 3. The comparison between computed and measured at 70 kJ: (a) Boulder impact force; (b) Maximum transmitted load along the horizontal centerline of the rigid barrier

Fig. 4. The split of right side boundary wall in DEM model for impact force measurement (all dimension in mm)

Fig. 5. Numerical model setup to investigate cushioning thickness: (a) $T_1/R_\mathrm{b} = 2$; (b) $T_2/R_\mathrm{b} = 3$;
(c) $T_3/R_\mathrm{b} = 5$

Fig. 6. Relationship between boulder impact force and average particle stress in force chains

Fig. 7. Energy profiles for a 1-m thick cushioning layer at 70 kJ

Fig. 8. Strain energy expansion angle at different time ($R_\mathrm{p}/R_\mathrm{b}$= 0.2): (a) t = 0.06 s; (b) t = 0.10 s (α: strain energy expansion angle)

Fig. 9. Strain energy expansion angle at different time ($R_\mathrm{p}/R_\mathrm{b}$ = 0.1): (a) t = 0.06 s; (b) t = 0.07 s (α: strain energy expansion angle)

Fig. 10. Effects of the radius ratio $R_\mathrm{p}/R_\mathrm{b}$ ranges from 0.1 to 0.5: (a) Maximum boulder impact force; (b) Maximum transmitted load; (c) maximum strain energy and friction energy

Fig. 11. Effects of cushioning thickness on the (a) Maximum boulder impact force; (b) Maximum transmitted load

List of Figures

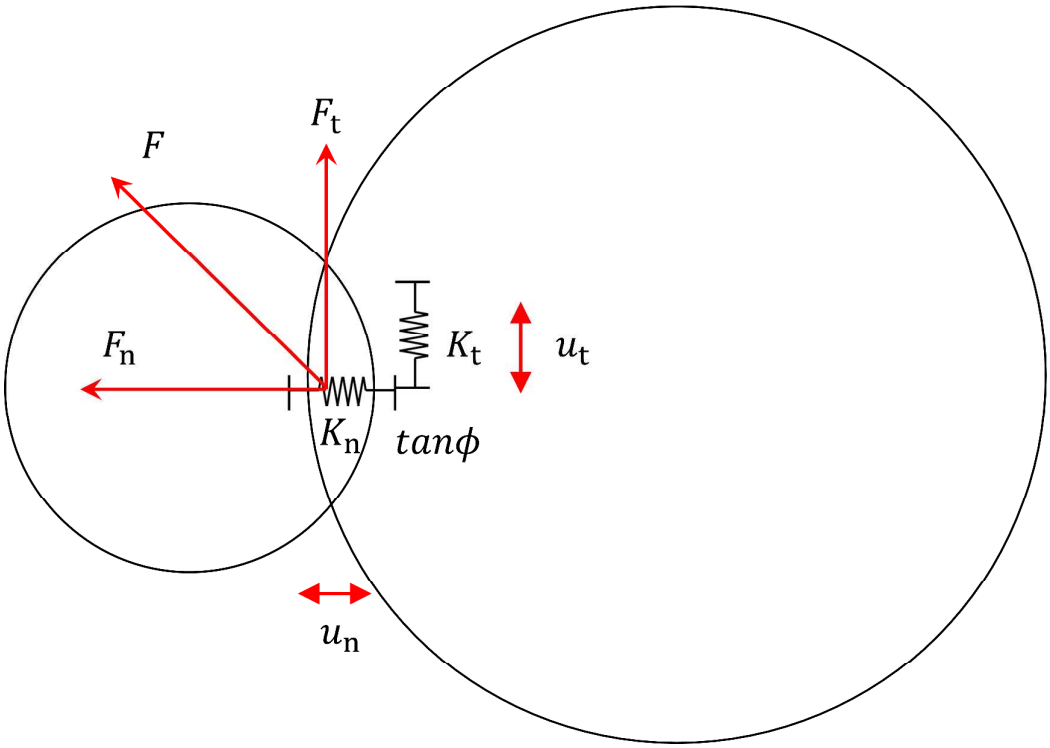

Fig. 1. Contact law of Hertz-Mindlin model.

(a)

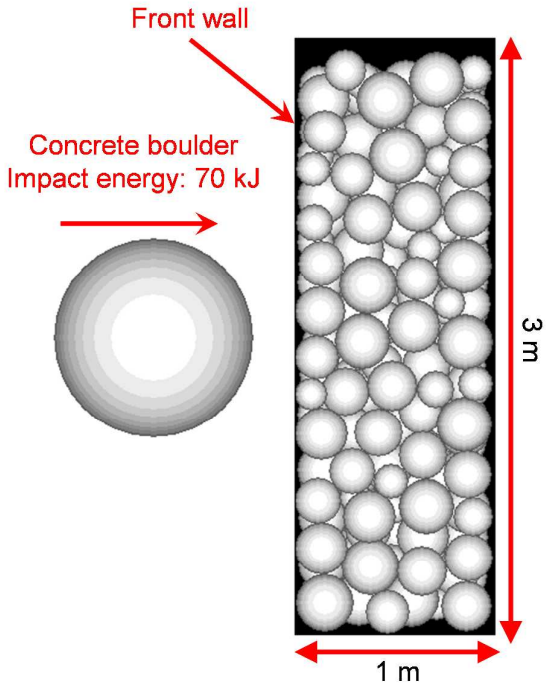

(b)

Fig. 2. Side view of test setup: (a) Physical test (Ng *et al.* 2016); (b) Numerical simulation

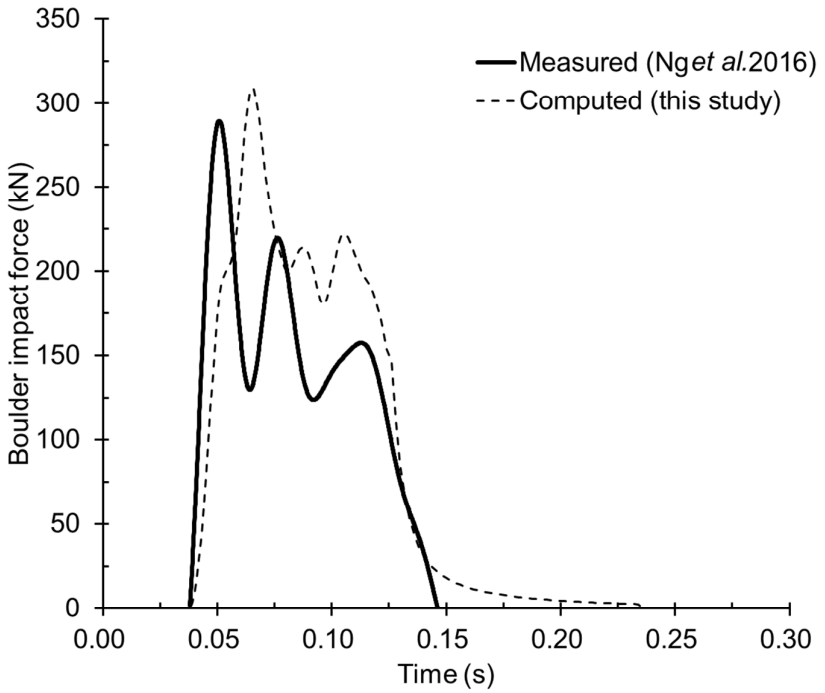

(a)

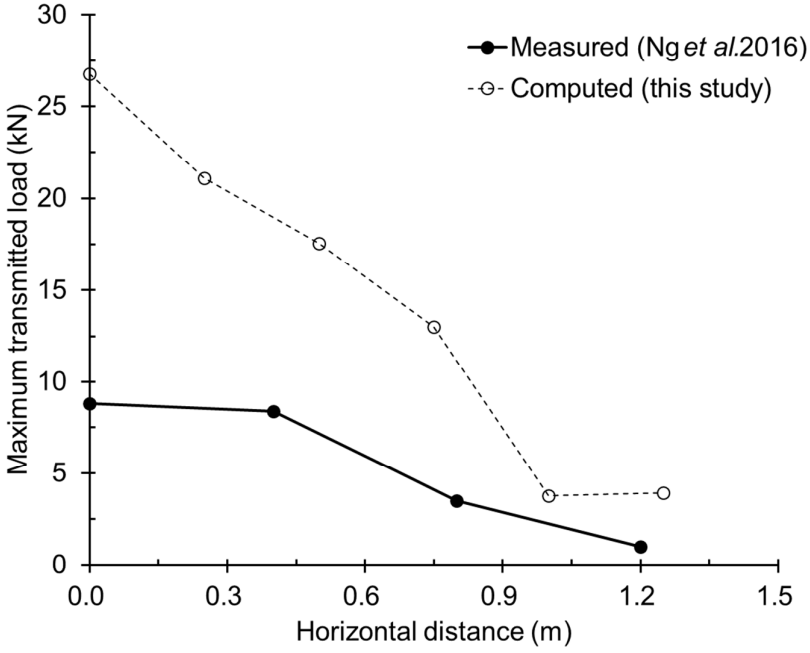

(b)

Fig. 3. The comparison between computed and measured at 70 kJ: (a) Boulder impact force; (b) Maximum transmitted load along the horizontal centerline of the rigid barrier

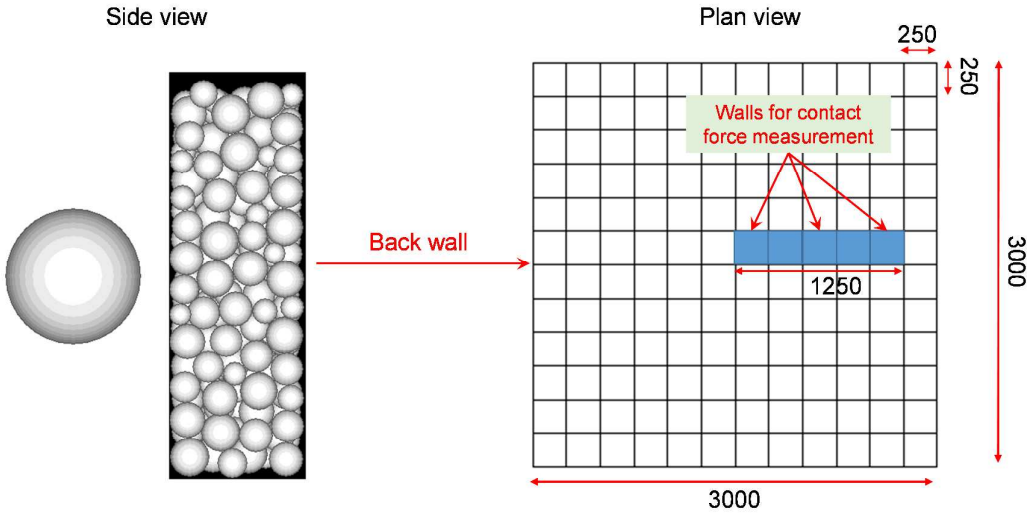

Fig. 4. The split of right side boundary wall in DEM model for impact force measurement (all dimension in mm)

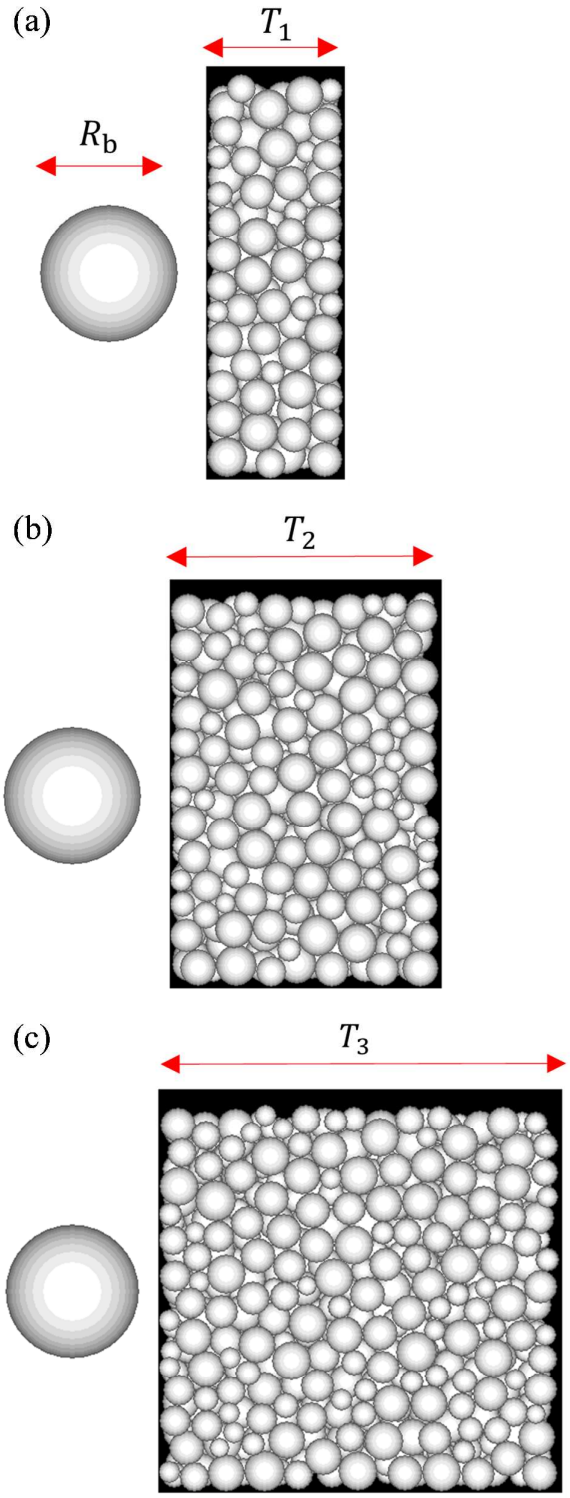

Fig. 5. Numerical model setup to investigate cushioning thickness: (a) $T_1/R_b = 2$; (b) $T_2/R_b = 3$; (c) $T_3/R_b = 5$

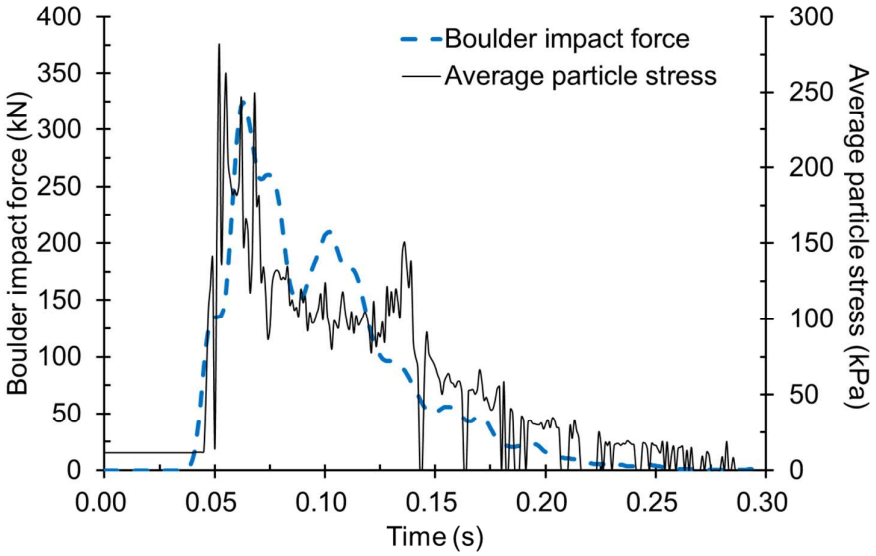

Fig. 6. Relationship between boulder impact force and average particle stress in force chains

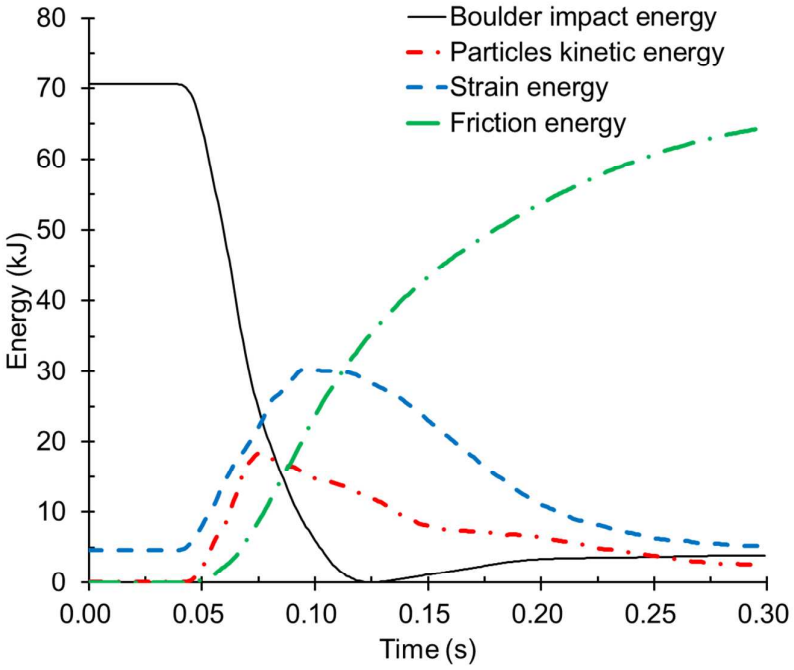

Fig. 7. Energy profiles for a 1-m thick cushioning layer at 70 kJ

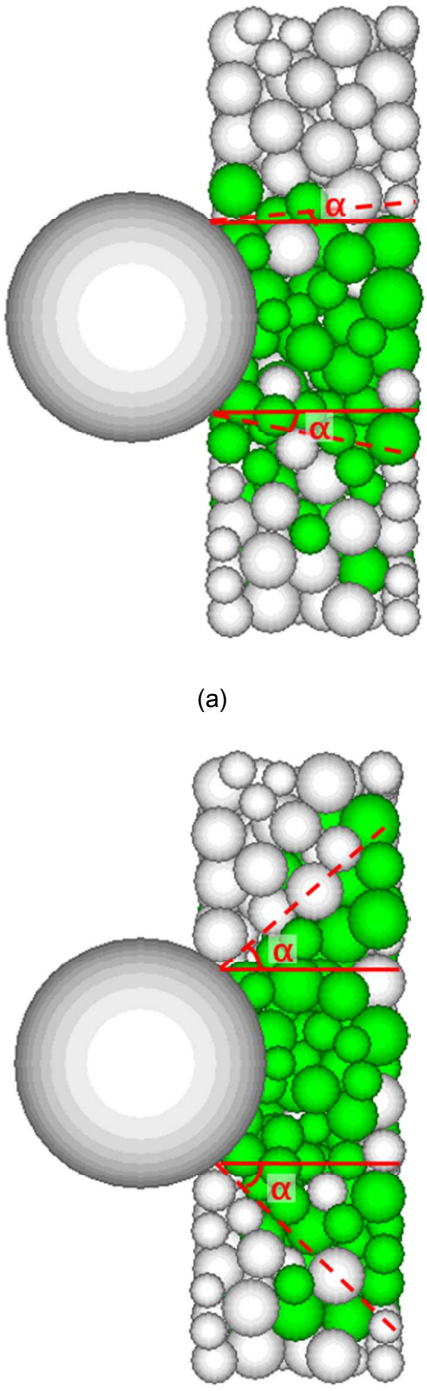

Fig. 8. Strain energy expansion angle at different time (R_p/R_b= 0.2): (a) t = 0.06 s; (b) t = 0.10 s
(α: strain energy expansion angle)

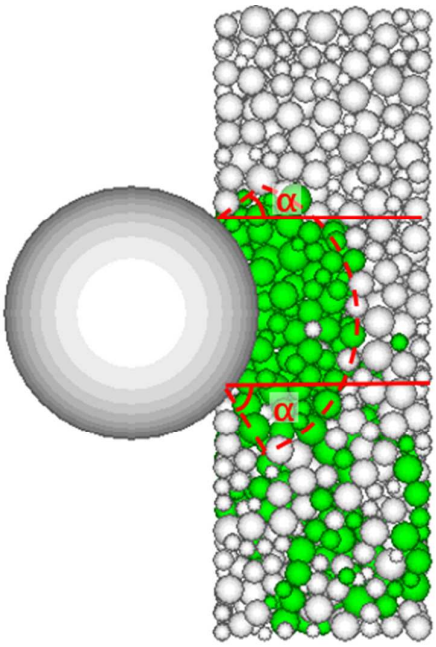

(a)

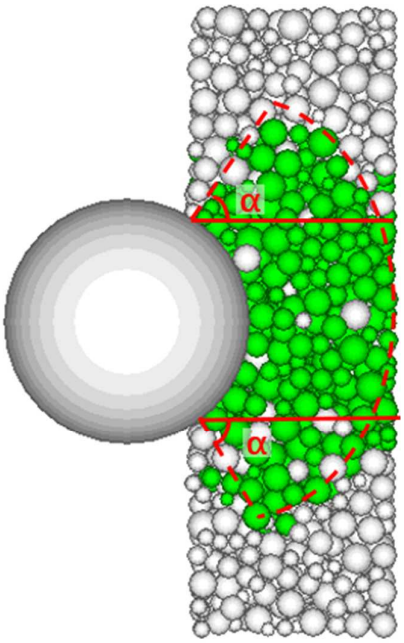

(b)

Fig. 9. Strain energy expansion angle at different time ($R_p/R_b = 0.1$): (a) $t = 0.06$ s; (b) $t = 0.07$ s

(α: strain energy expansion angle)

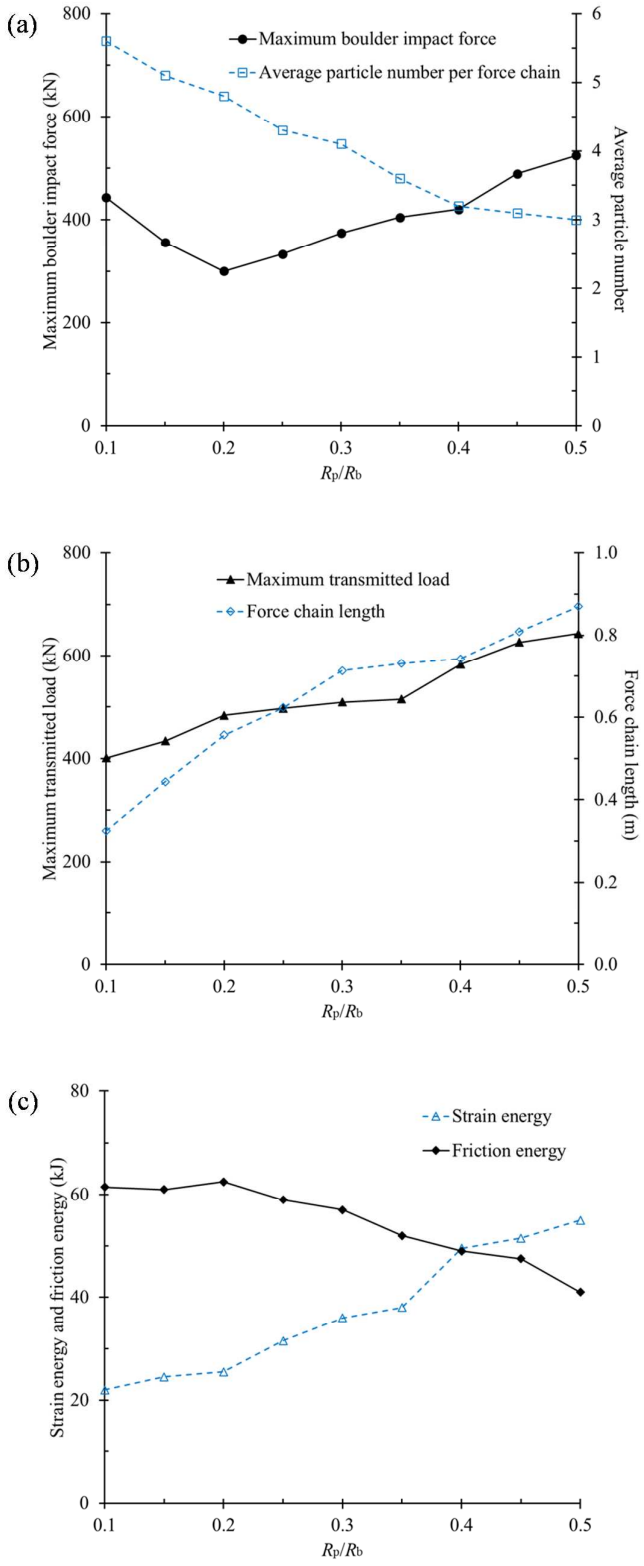

Fig. 10. Effects of the radius ratio R_p/R_b ranges from 0.1 to 0.5: (a) Maximum boulder impact force; (b) Maximum transmitted load; (c) maximum strain energy and friction energy

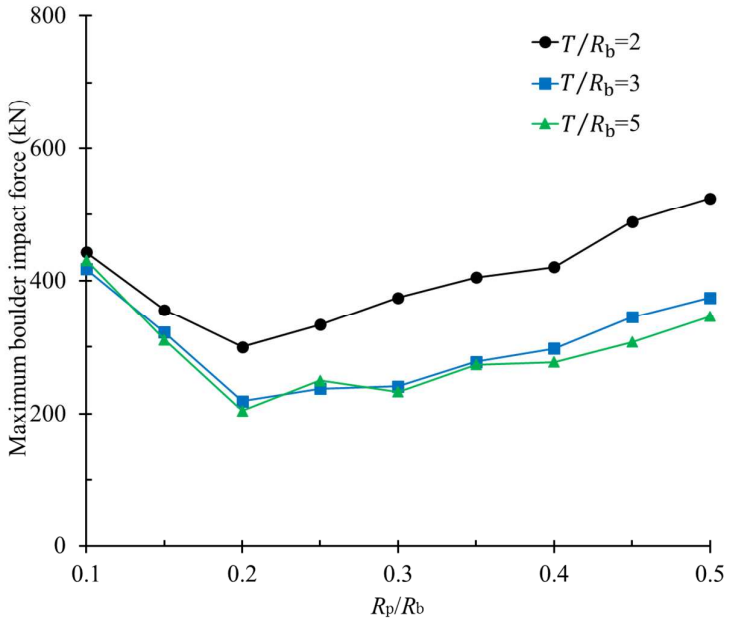

(a)

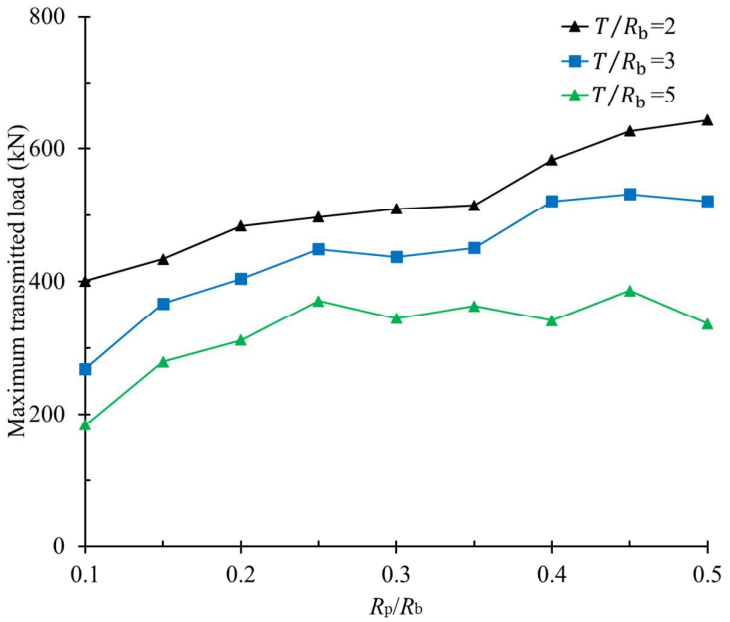

(b)

Fig. 11. Effects of cushioning thickness on the (a) Maximum boulder impact force; (b) Maximum transmitted load

Table 1 Adopted particle size and cushion thickness in the field (Heymann *et al.* 2011; Lambert *et al.* 2009; 2014; Ng *et al.* 2016)

References	Particle size (mm)	Cushion thickness (m)
Lambert *et al.* 2009	60-180	0.5
Heymann *et al.* 2011	80-120	3
Lambert *et al.* 2014	80-120	2
Ng *et al.* 2016	160-300	1

Table 2 DEM Model parameters used in current study

Parameters	Values
Gravity (m/s^2)	9.8
Density (kg/m^3)	2650
Shear modulus (MPa)	2×10^7
Poisson's ratio	0.25
Local friction angle (deg)	30
Normal damping coefficient	0
Porosity	0.4

Table 3 Summary of parameters used in parametric study

Particle radius ratio (R_p/R_b)	Thickness ratio (T/R_b)
0.10, 0.11, 0.13, 0.14, 0.15,	2
0.17, 0.20, 0.25, 0.30, 0.33,	3
0.35, 0.40, 0.45, 0.50	5